Journal Name

ARTICLE

Received 00th January 20xx,
Accepted 00th January 20xx

DOI: 10.1039/x0xx00000x

www.rsc.org/

Polyelectrolyte interlayers with a broad processing window for high efficiency inverted organic solar cells, towards mass production

Chen Wang,[a] Roderick C. I. MacKenzie,[b] Shanpeng Wen,*[a] Yang Liu,[c] Pengfei Ma,[a] Chang Li,[a] Ge Wang,[a] Wenjing Tian[c] and Shengping Ruan[a]

Neutral polyelectrolyte interfacial layers in organic solar cells are well-known for their ability to tailor the work function of electrodes, improve charge carrier extraction and maximize open circuit voltage. However, they also suffer from low charge carrier conductivity, therefore the interlayer must be kept thin, which in turn requires very precise deposition. This prerequisite significantly reduces the robustness of the fabrication process, and makes such structures difficult to up-scale for roll-to-roll mass production. Herein, we find that by washing the polyelectrolyte layer with N,N-Dimethylformamide (DMF) after deposition, solar cell efficiency jumps to near optimum levels, no matter what the original thickness of the polyelectrolyte layer. Subsequent characterization of the DMF-washed ZnO/PEI interlayer reveals a changed surface structure, passivated surface trap states, thus improved transport properties and lower recombination losses. We demonstrate the general applicability of the method to other state-of-the-art material systems, namely P3HT:ICBA, PTB7:$PC_{71}BM$ and PTB7-Th: $PC_{71}BM$. We find the more efficient the material system, the larger the improvement in efficiency after DMF washing. Thus, this method represents a general way to relax the fabrication criteria for high efficiency organic solar cells. We anticipate this method could be of use in other classes of devices such as OTFTs and OLEDs.

1. Introduction

Organic photovoltaic devices (OPVs) offer a potentially low cost,[1] low carbon,[2] and environmentally safe[3] way to generate electricity from solar radiation. Over the last decade, power conversion efficiencies (PCEs) have risen from 3% in 2003, to over 11% today.[4-8] While at the same time, lifetimes have also risen from minutes to hundreds of days.[9-11] These advances, have been achieved through development of new narrow bandgap polymers such as, PTB7,[12] PTB7-Th,[13] PffBT4T-2OD,[14] and PBDB-T[15] and through the deployment of inverted device structures. Inverted geometries take advantage of vertical phase separation in active layer and also reduce the cells ability to react with oxygen/water.[16-18]

Efficient light absorbing polymers and inverted cell structures are not the only two advances enabling these encouraging results, there have also been significant advances in interface engineering which allow photo-generated charge carriers to leave the device efficiently. Ideally optimized contact and buffer layers provide well aligned energy levels and good physical contact to the active layer, so as to minimize the barrier to charge extraction.[19,20] It has been demonstrated that by depositing aluminium with high work function n-type MoO_3,[21] ohmic anode contacts can be formed.[15,22,23] For the cathode on the other hand, transparent indium tin oxide (ITO) is commonly used, which possesses a work function significantly higher (≈ 4.7 eV)[24] than that of the lowest unoccupied molecular orbital (LUMO) of fullerene acceptors $PC_{61}BM$ (≈ 3.9 eV)[25] or $PC_{71}BM$ (≈ 4.0 eV).[26] Therefore, developing ITO modifiers that match the LUMO level of PCBM is desirable. In this regard, inorganic n-type transition metal oxides (e.g. ZnO, TiO_2 and SnO_2) have been explored as they theoretically possesses ideal energy level (≈ 4.0 ~ 4.2 eV) alignment to PCBM, as well as

[a] State Key Laboratory on Integrated Optoelectronics and College of Electronic Science & Engineering, Jilin University, Changchun 130012, P. R. China.
[b] Faculty of Engineering, The University of Nottingham, University Park, Nottingham, NG7 2RD, UK.
[c] State Key Laboratory of Supramolecular Structure and Materials, Jilin University, Changchun 130012, P. R. China.
E-mail: sp_wen@jlu.edu.cn

† Electronic Supplementary Information (ESI) available: Supplementary figures. See DOI: 10.1039/x0xx00000x

relatively high electron conductivity.[27-28] However, due to impurities introduced during production/deposition of these materials the actual work functions values are often non optimal for electron extraction from PCBM component.[29,30] Furthermore the surface of these oxides often contain impurities/defects, which can act as traps for charge carriers and thus hinder transport into the material.[31,32] To overcome these problems, surface modifiers designed to fine tune the energy levels of the metallic oxide surface and reduce electron trapping have been investigated, these include polyelectrolyte-type materials,[33,34] self-assembled monolayers[35] and fullerene-based interlayers.[13,36] The inexpensive and charge neutral polyelectrolyte of polyethylenimine (PEI) or polyethylenimine-ethoxylated (PEIE) has been shown able to reduce the work function at the ZnO surface, by the formation of an interface dipole moment.[37] Efficiency increases of over 25% for polymer[24] and small-molecule[38] based solar cells have been observed by using this approach. However, these modified layers have their own drawbacks, that is, the PEI is intrinsically insulating and the film needs to be kept thin to achieve good performance.[24] This need for accurate control over layer thickness, is highly problematic from the view of scale-up and reproducibility (even on a lab scale).[39] Therefore, before such devices can be considered for mass production, the need for exact control over the PEI layer, must be relaxed.

In this work, we first optimize an inverted cell using PEI to modify the ZnO cathode buffer layer. It is demonstrated that the application of PEI can raise open-circuit voltage (V_{oc}), short-circuit current density (J_{sc}) and fill factor (FF) simultaneously, thus leading to an efficiency enhancement of at least 30%. We then investigate using N,N-Dimethylformamide (DMF) to treat the already deposited PEI layers. We observe that after the application of DMF, all devices, no matter how thick the initial PEI layer, demonstrate almost optimal PCEs. The application of DMF can help to re-dissolve and spread the PEI. This thins the PEI and also guarantees surface coverage/film uniformity, enabling the PEI to fill the surface defect states of the ZnO layer. Consequently, the PEI/DMF based device affords more favourable transport and recombination behaviour. This methodology is applied to devices containing different light absorbing polymers, including PTB7, PTB7-Th, P3HT and PDTS-DTffBT. Thus, we demonstrate that DMF washing acts as a general method to broaden the parameter window of PEI interlayers, and make device fabrication a more robust. Interestingly, we find the more efficient the material system the larger the impact DMF washing has on device efficiency.

2. Results and discussion

2.1 Device fabrication and cell performance

The chemical structures of materials, and inverted device structure used in this study are depicted in Fig. 1. The structure comprises of a glass ITO substrate, onto which, the ZnO film thermally decomposed at 150 °C (left). This temperature is low enough that flexible substrates will not be melted.[29] The branch PEI buffer layer and photoactive layer were spin-cast, followed by thermal deposition of the molybdenum trioxide/silver (MoO_3/Ag) anode. For the devices, where the PEI layer was treated with DMF, 200 μL DMF at 70 °C was pipetted onto the PEI-coated substrate and spun off immediately. A blend of poly{4,4′-bis(2-ethylhexyl)dithieno[3,2-b:2′,3′-d]silole-alt-5,6-Difluoro-4,7-bis(4-hexylthiophen-2-yl)-2,1,3-benzothiadiazle} (PDTS-DTffBT) and $PC_{71}BM$ were used to form the active layer. PDTS-DTffBT is a low band-gap polymer developed by the current authors.[40] For the model devices, we changed the PEI concentration from 0.05 wt% to 1.6 wt%, to vary the thickness of the PEI layer, and understand the impact of thickness on device performance. We then repeated this set of experiments, but applied the DMF to the PEI layer.

Fig. 2 displays the corresponding current density-voltage (*J*-*V*) curves for the inverted solar cell structures (ITO/ZnO/PEI/PDTS-DTffBT:$PC_{71}BM$/MoO_3/Ag) with varying PEI concentrations under AM 1.5 G illumination. To ensure reproducible and reliable results, each time an experimental variable was altered, 5 devices were fabricated and tested individually. The results, along with a statistical summary of repeatability can be found in Table 1. A device with no PEI layer was also fabricated to act as a reference device (this can be seen in Fig. 2), it has an V_{oc} of 0.67 V, J_{sc} of 12.57 mA cm^{-2}, FF of 53.4% and a modest PCE of 4.5%. This result is around 2% below the champion, device with a PEI layer, which had a PCE of 6.41%, V_{oc} of 0.73 V, J_{sc} of 13.72

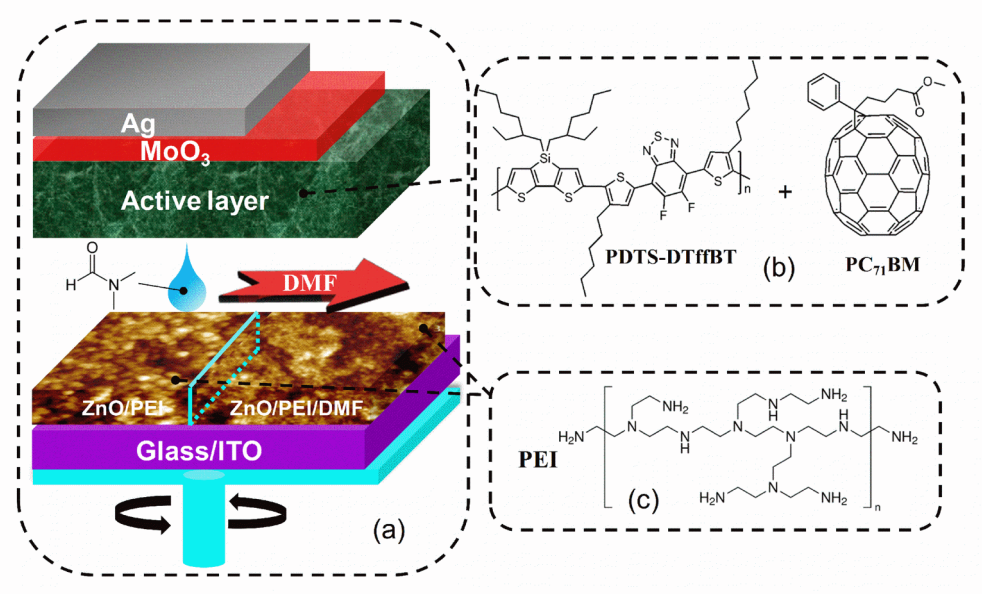

Fig. 1 Illustration of device structure, DMF treatment and chemical structures of the materials used.

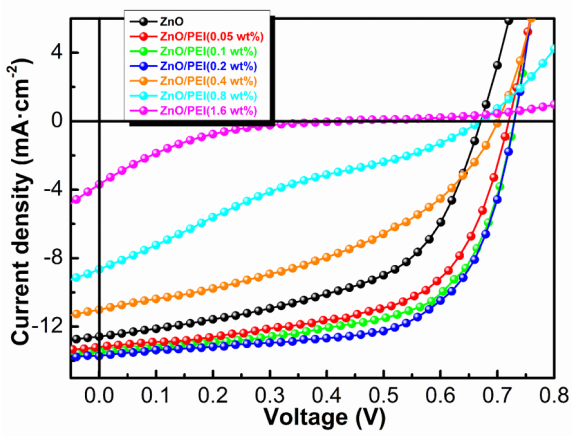

Fig. 2 J-V curves of PDTS-DTffBT based solar cells without or with PEI modifier at different PEI concentration.

mA cm^{-2} and FF of 64%. We found the optimal, concentration of PEI to be 0.2 wt%. Concentrations of PEI lower than 0.2 wt %, were found not to be detrimental to device performance, while concentrations higher than 0.2 wt% were found to quickly degraded performance, probably due to the insulating properties of the layer. To the best knowledge of these authors, this is the first time that the V_{oc} and FF, have been tuned by exactly varying the layer thickness of a PEI on ZnO.

It can be seen from the above results, that a 2% increase in device efficiency can be obtained by adding a PEI layer, however the thickness of this layer must be controlled to within 3 nm. The PEI thickness is determined by Ellipsometry, and will be explained in detail later. Controlling the thickness of a layer to this accuracy in the lab for a small area device is possible but difficult, however doing this for mass production would be a much more difficult and expensive challenge. Therefore, next we attempt to relax the requirements for precise thickness control by washing the PEI layer, post deposition with DMF. We spin 200 µL of DMF at 70 °C on top of the PEI layer, the sample is then annealed on hot plate for 10 min at 100 °C. Fig. 3a plots the *J-V* curves of devices with non-optimal (thick) PEI layers, made using 0.4 (red), 0.8 (green) and 1.6 wt % (blue) solutions. It can be seen that the, *J-V* curves from these devices are far from optimal displaying characteristic S-shape behavior with poor fill factors. Then plotted on the Fig. 3b, are three *J-V* curves which are from devices nominally identical to those in Fig. 3a except, before deposition of the BHJ, the PEI layer was washed with DMF. It can be seen that all three devices washed with DMF display optimal *J-V* curves. The 0.8 wt% PEI based devices, after DMF treatment, gave even better device metrics of V_{oc} of 0.73±0.01 V, J_{sc} of 14.00±0.07 mA cm^{-2}, FF of 63.9±0.3% and maximum PCE of 6.57% than the the champion results when only using an unwashed PEI layer. Detailed device metrics can also be found in Table 1.

2.2 Understanding the physical washing mechanism

To understand how PEI and DMF interact with the ZnO surface we use a combination of Ellipsometry, Fourier transform infrared spectroscopy (FTIR), X-ray photoelectron spectroscopy (XPS), Photoluminescence (PL), Surface contact angle measurements and Ultraviolet photoelectron spectroscopy (UPS). First, the FTIR spectra of PEI, DMF and PEI treated DMF are first shown in Fig. 4. By comparing all three spectra, it can be seen that the PEI treated DMF spectra contains (shifted) absorption bands from both the PEI and DMF. Specifically, the sharp absorption band from the C=O bond of DMF at 1679 cm^{-1}, can be seen to have been down shifted to 1661 cm^{-1} in the PEI/DMF sample. The vibrations from the N-H amine moiety of PEI, broaden at around 3300 cm^{-1} and up shift at 1589 cm^{-1}. These observations suggest formation of intermolecular hydrogen-bonds between the amine group in PEI and carbonyl group in DMF,[41] it is unlikely that the DMF ever fully leaves the film and thus is expected to influence the deposition and formation of the BHJ.

We noticed that, when a PEI surface was washed with hot DMF solvent, the PEI became soft and spread out to form a more uniform and smooth surface. Therefore, at this point we

speculate that there is a surface thinning and re-construction process take place. In order to test our assertion, the properties of ZnO/PEI layer were measured by atomic force microscopy

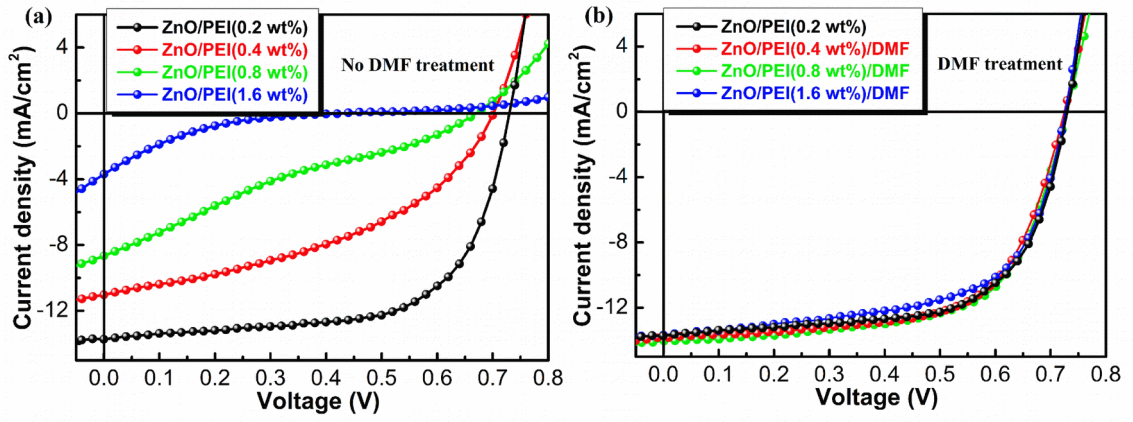

Fig. 3 The *J-V* curves of devices using high concentration PEI before (a) and after (b) DMF treatment.

Table 1. *J-V* performance parameters of PDTS-DTffBT based PSCs adopting different interfacial layers.

Interfacial layer	PEI thickness (nm)	V_{oc} (V)	J_{sc} (mA/cm²)	J_{sc}^{EQE} (mA/cm²)	FF (%)	PCE (%)	
						Max.	Aver.
ZnO	-	0.67±0.01	12.43±0.21	11.60(7.7%)	53.5±1.1	4.50	4.45
ZnO/PEI(0.05 wt%)	1.77	0.72±0.01	13.21±0.24	12.33(6.5%)	59.2±0.9	5.68	5.63
ZnO/PEI(0.1 wt%)	2.72	0.73±0.01	13.52±0.06	12.67(6.1%)	62.4±0.4	6.15	6.12
ZnO/PEI(0.2 wt%)	3.01	0.73±0.01	13.75±0.13	12.92(6.0%)	63.3±0.5	6.41	6.35
ZnO/PEI(0.4 wt%)	7.50	0.71±0.01	10.92±0.14	10.20(7.4%)	42.8±0.2	3.32	3.29
ZnO/PEI(0.8 wt%)	13.41	0.67±0.01	8.66±0.18	8.03(6.8%)	21.5±1.4	1.25	1.22
ZnO/PEI(1.6 wt%)	22.08	0.44±0.02	3.69±0.22	3.39(7.7%)	12.1±1.7	0.19	0.17
ZnO/PEI(0.05 wt%)/DMF	1.17	0.72±0.01	13.19±0.26	12.40(6.8%)	60.5±0.6	5.80	5.71
ZnO/PEI(0.1 wt%)/DMF	1.66	0.73±0.01	13.59±0.05	12.67(6.6%)	62.6±0.4	6.22	6.17
ZnO/PEI(0.2 wt%)/DMF	2.20	0.73±0.01	13.71±0.04	12.74(7.1%)	63.4±0.7	6.40	6.30
ZnO/PEI(0.4 wt%)/DMF	5.99	0.73±0.01	13.80±0.08	12.90(6.5%)	62.9±0.3	6.39	6.32
ZnO/PEI(0.8 wt%)/DMF	9.43	0.73±0.01	14.00±0.07	13.11(6.5%)	63.9±0.3	6.57	6.51
ZnO/PEI(1.6 wt%)/DMF	11.97	0.73±0.01	13.62±0.13	12.88(5.7%)	61.5±0.3	6.15	6.09

(AFM) and Ellipsometry. Fig. 5, plots AFM images of the surface of ZnO, ZnO/PEI(0.2 wt%), ZnO/PEI(0.8 wt%) and ZnO/PEI(0.8 wt%)/DMF. It can be seen that both the ZnO and the ZnO/PEI(0.2 wt%) samples have a similar blotchy surface pattern, and a roughness of 1.61 nm and 1.45 nm respectively, this suggests that PEI is not uniformly covering surface but is instead forming a network of inter-linked islands.[37] In contrast the ZnO/PEI(0.8 wt%) film, it shows a uniform and more detailed herringbone like structure. Once the ZnO/PEI(0.8 wt%) film is washed with DMF, this detailed pattern is washed away and the blotchy appearance of the ZnO substrate reappears,

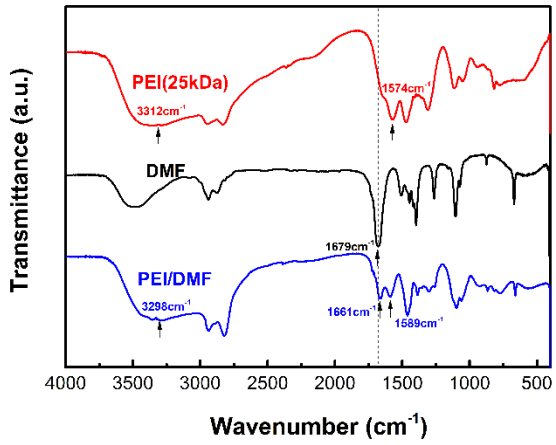

Fig. 4. The FTIR spectra of PEI, DMF and the PEI/DMF. It can be seen that the PEI washed DMF sample contains absorption bands from both the PEI and DMF spectra, suggesting hydrogen bond formation.

however it has a lower roughness of 0.96 nm, and appears more gently undulating than the ZnO/PEI(0.2 wt%). This suggests that some of the PEI has been washed away, and a thinner more smooth covering of PEI has been left behind.

We further deposit PEI solutions of between 0.05 wt% and 1.6 wt% on Si/ZnO substrates to understand how DMF washing affects the thickness of the PEI film. We perform Ellipsometry to obtain the final PEI film thickness. The results are shown in Table 2, the Ψ fitting in Ellipsometry analysis has been shown in Fig. S1. It can be seen that after DMF washing a decrease in PEI film thickness can be seen. It is interesting to note that the thicker the film, the larger the reduction in film thickness. Despite PEI's beneficial modification to the band structure, it is never the less an insulating material and too thick a layer would be expected to prevent charge carrier extraction and cause S-shaped *J-V* curves. Thus, the thinning of the layer by DMF can be seen as beneficial to device performance.

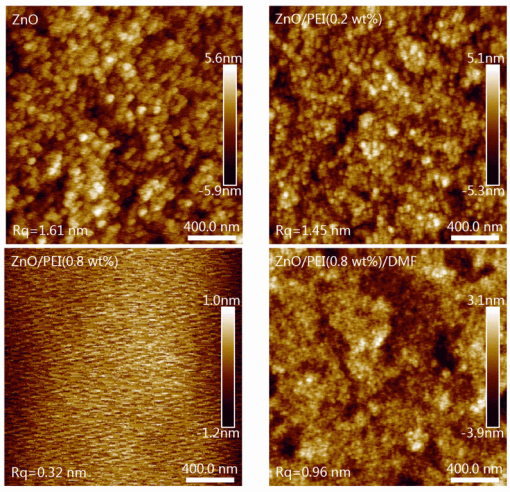

Fig. 5. The AFM height images (2μm×2μm) of ZnO, ZnO/PEI(0.2 wt%), ZnO/PEI(0.8 wt%) and ZnO/PEI(0.8 wt%)/DMF on the ITO substrate.

Table 2. Thicknesses of the PEI films before and after washing with DMF, as measured by Ellipsometry

	0.05wt %	0.1wt %	0.2wt %	0.4wt %	0.8wt %	1.6wt %
Si/ZnO/PEI	1.77	2.72	3.01	7.50	13.41	22.08
Si/ZnO/PEI/DMF	1.17	1.66	2.20	5.99	9.43	11.97

To further understand these physical changes, we use XPS to study the changes in surface chemistry. Fig. 6 shows plots of the narrow scan of N1s, Zn2p and O1s core level spectra. We note that when PEI is deposited on ZnO substrate, the N1s double peaks changes into single peak, and the peak of the spectra shifts towards a high binding energy while, the Zn2p spectra shifts to lower binding energies. This suggests that the electron-rich amine groups in the PEI interact with ZnO surface and form N-Zn bonds by slight electron transfer.[37,42,43] After treating the ZnO/PEI film with DMF, the N1s binding energy can be seen to further increase while the Zn2p binding energy further decreases in magnitude. This indicates more Zn atoms are bound to N atoms and decreases the number of under-coordinate atoms. This suggests better surface coverage of the ZnO by the PEI and is consistent with the above morphological features.

Fig. 7 plots the PL emission from pristine ZnO, ZnO/PEI and ZnO/PEI/DMF. It can be seen that pristine ZnO gives the largest PL signal, while coating in PEI reduces the signal. We find washing the PEI with DMF further reduces the PL signal. We attribute the ZnO surface defects to uncoordinated zinc atoms and oxygen states, these types of defects are commonly found in sol-gel deposited at low temperature.[29,42,44] Both theory and experiment have previously been used to demonstrate that these states are the main reason for the broad green luminescence of ZnO.[31,45-48] In our work, the surface defects of ZnO are also seen in the XPS data. After PEI modification and DMF treatment, the N1s peak shifts towards a high binding energy while Zn2p spectra shift to lower binding energies. This indicates more Zn atoms are bound to Nitrogen atoms and thus PEI/DMF is effectively passivating these emissive states.

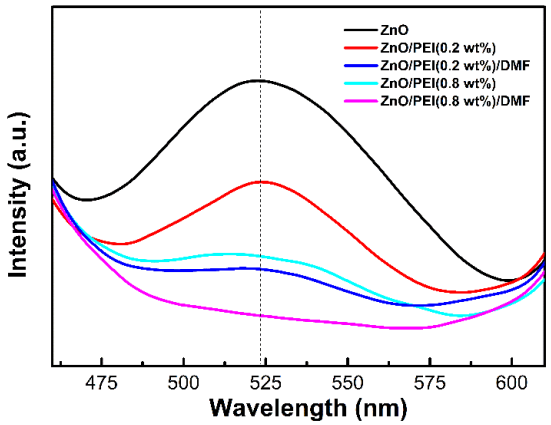

Fig. 7. The PL spectra of oxygen defects on the ZnO surface. As the layer thickness of PEI is increased, the PL signal drops. This indicates that surface defects are being passivated by the PEI film. On application of DMF, the PL signal drops further indicating improved surface coverage.

To understand how the application of PEI and DMF washing affects the work function and band structure of the device, we performed UPS measurements; the results are plotted in Fig. S2a. We can see that the work functions of films at the surface are, 4.17 eV for ZnO, 4.01 eV for ZnO/PEI and 3.96 eV for ZnO/PEI/DMF, applying the PEI lowers the work function by around 0.2 eV. We attribute the reduced work function of the ZnO/PEI film to the formation surface dipoles within PEI.[37] It can be seen that, both the ZnO/PEI and ZnO/PEI/DMF films have work functions considerably lower than that of the bare ZnO film. However, the difference in

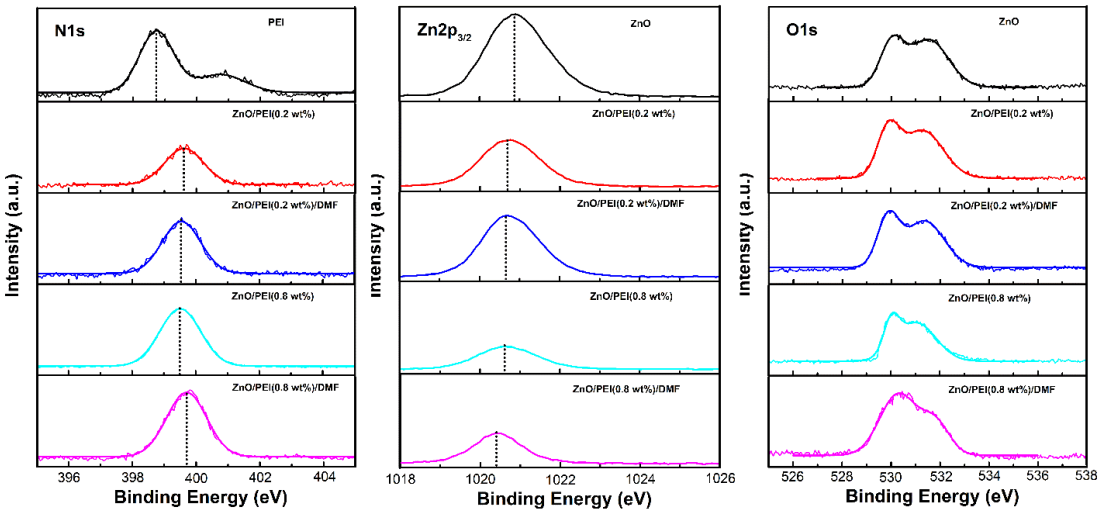

Fig. 6. The XPS narrow scan of N1s, Zn2p and O1s core level spectra of different sample.

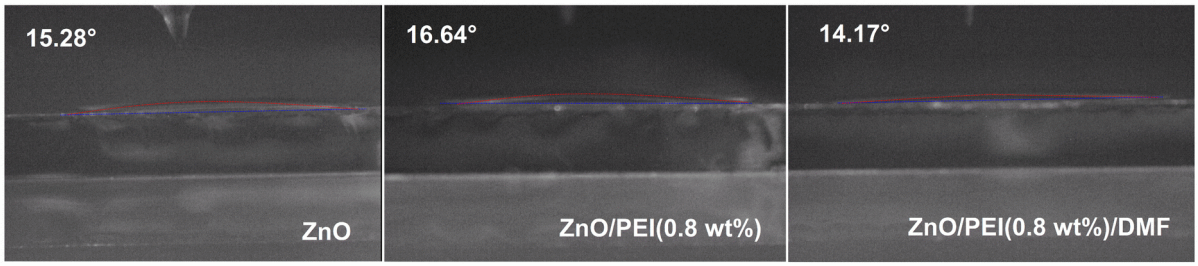

Fig. 8. Contact angle of chlorobenzene on the surface of ZnO, ZnO/PEI and ZnO/PEI/DMF samples.

energy level between the ZnO/PEI and the ZnO/PEI/DMF films is small, suggesting the application of DMF does not significantly affect the energy level diagram of the device (see Fig. S2b).

It is possible, that part of the reason for the improved electrical performance is a better physical contact between the active layer and the interlayer. To investigate if this, we use surface contact angle measurements to examine the wetting between chlorobenzene, and the ZnO, ZnO/PEI and ZnO/PEI/DMF surfaces (the active layer is dissolved in chlorobenzene). The results are shown in Fig. 8, where it can be seen that the ZnO/PEI/DMF sample has a slightly lower contact angle than the other two films. This lower contact angle, would be expected to result in better wetting between the active layer and the contact during fabrication, resulting in better physical contact between the two layers and lower electrical resistance.

In summary, the application of PEI to ZnO lowers its work function which is beneficial for the electrical performance of the device. While application of DMF to the PEI layer helps to re-dissolve and spread the PEI. This thins the PEI while guarantees the surface coverage/film uniformity, enabling the PEI to fill the surface defect states of the ZnO layer and work better even for thicker layers. In addition, the application of DMF also potentially result in better physical contact between the two layers and thus lower electrical resistance.

2.3 Electrical characterisation of the devices

To understand how DMF-washing affects charge extraction and recombination dynamics in the devices, we apply the Transient Photocurrent (TPC), Transient Photovoltage (TPV), Charge Extraction by Linear Voltage (CELIV) and Impendece Spectrocopy techniques.[49,50] In TPC and TPV measurments, a short laser pulse (10 ns) is used to photo-excited the device. In a TPC measurement, the device is kept at short circuit, and the photogenerated carriers are swept out of the device by drift and/or diffusion. This measurement technique can be used to (amongst other things) measure carrier extraction efficiency and transport. Conversely, in TPV measurements, the device is kept at open circuit and the change in open circuit voltage monitored after the laser pulse. The decay rate of the voltage transient has

been linked to the recombination rate.[51] It is important to note that both these techniques are small signal perturbation techniques, meaning that changes to V_{oc} and J_{sc} are kept to below about 5%. Fig. 9 shows the TPC and TPV transients measured from devices based on ZnO, ZnO/PEI and ZnO/PEI/DMF.

From Fig. 9a, it can be seen that the devices with the PEI, have a higher peak to their current transient suggesting better photogeneration, the transients also decay more quickly suggesting better transport out of the device.[52] The characteristic times of the ZnO, ZnO/PEI, and ZnO/PEI/DMF transients are, 1.69 μs, 1.22 μs and 1.21 μs respectively. From Fig. 6b, which depicts the TPV transients at 1 Sun, it can be seen that the transient from the ZnO based device decays more quickly than those of the device with the interlayers present. By fitting the equation:[51]

$$\Delta V_{OC}(t) = \Delta V_{OC0} e^{\frac{-t}{\tau_{\Delta n}}}$$

to the transients, the charge carrier lifetime can be estimated as 3.47 μs, 4.27 μs and 4.85 μs for the devices with ZnO, ZnO/PEI, and ZnO/PEI/DMF layers respectively. This suggests that

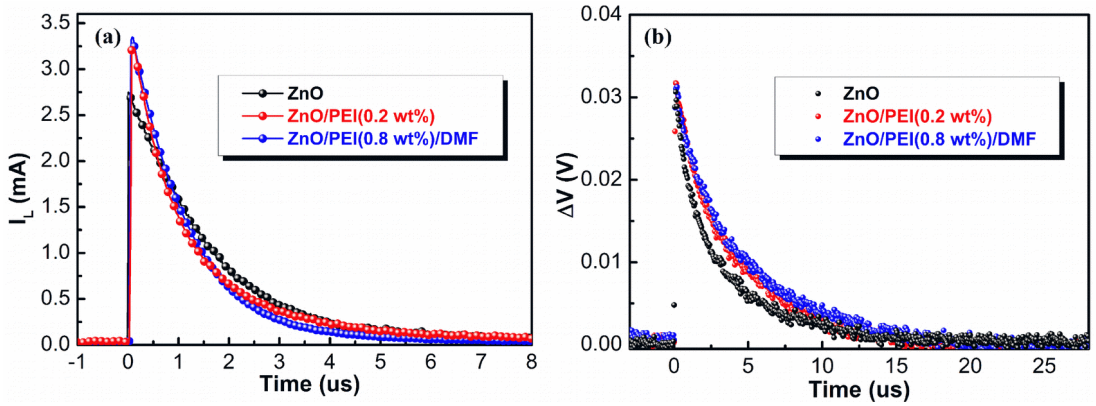

Fig. 9. The TPC (left) and TPV (right) analyses of working devices based on ZnO, ZnO/PEI and ZnO/PEI/DMF.

recombination in ZnO/PEI/DMF device is the slowest. These suppressed recombination losses will contribute to the higher V_{oc}s experimentally observed in the optimal ZnO/PEI and ZnO/PEI/DMF devices.

To further understand the effect of the PEI interlayer on charge carrier transport we use the Carrier Extraction by Linearly Increasing Voltage (CELIV) technique.[53] We found that device mobility as extracted by CELIV increased from 8.9×10^{-5} cm^2/Vs for a device with no PEI layer to 2.53×10^{-4} cm^2/Vs for a device with a PEI layer. For a device with a PEI/DMF interlayer mobility was found to be 5.24×10^{-4} cm^2/Vs. It is important to note that CELIV will measure the mobiluty of the entire device not just the active layer, thus these values probably represent better charge carrier extraction at the ZnO contact. These experiments and resulting CELIV curves are discussed in detail in the SI (Fig. S3).

Finally, to further understand the electrical performance of the interface, impedance spectroscopy was used under dark conditions to measured the frequency response of the cells from 20 Hz to 1 MHz. Nyquist plots of the PEI-based devices (0.2 wt %, 0.8 wt%, 0.8 wt%/DMF) are shown in Fig. 10. It can be seen that both the Re(Z) and Im(Z) values are significantly increased when using 0.8 wt%-PEI, indicating a larger resistance of the device caused by the thick PEI layer. While after DMF treatment, the impedance spectrum recovers and shows smaller semi-circle than the 0.2 wt%-PEI coated device. To interpret the impedance spectra, the data was fit by an equivalent circuit (see Fig. 10 inset), the fitting parameters are summarized in Table 3. We take the element R_0 as representing the series resistance of the device, elements R_1C_1 representing the electrodes, while elements R_2C_2 represent the active layer.[54-56] From this analysis we observed an increase in both R_1C_1 and R_2C_2 elements of 0.8 wt%-PEI device and recovery after solvent treatment. Since these devices have an identical anode contact, it suggests that the DMF washing decreased cathode interfacial resistance, which prevents the formation of a charge extraction barrier and facilitates charge transport.

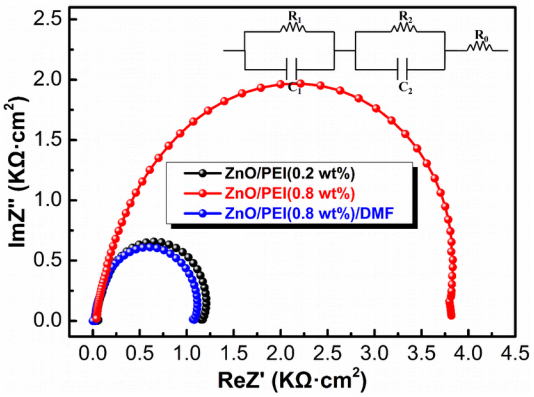

Fig. 10. The Nyquist plots of devices based on different PEI concentration and DMF treatment. The inset is corresponding RC equivalent circuit model.

Table 3. The values of R and C used to fit the measured impedance data.

Device	R_0 (Ω·cm²)	R_1 (Ω·cm²)	C_1 (nF)	R_2 (Ω·cm²)	C_2 (nF)
ZnO/PEI(0.2 wt%)	33	1277	39	158	7.4
ZnO/PEI(0.8 wt%)	40	3693	41	161	7.2
ZnO/PEI(0.8 wt%)/DMF	34	1206	37	151	6.9

2.4 Generalization of the method to other material systems

Above, we have demonstrated that treatment of a PEI interlayer with DMF, is beneficial for a device with a PDTS-DTffBT/$PC_{71}BM$ active layer. We now demonstrate the general applicability of DMF washing to a series of devices with different active layers. The *J-V* curves of three devices based on P3HT:ICBA, PTB7:$PC_{71}BM$ and PTB7-Th: $PC_{71}BM$ are shown in Fig. 11 (metrics are available in Table 4). It can be seen for all devices, washing with DMF increased performance. For the P3HT:ICBA system, before DMF washing, a PCE of 5.19% and a V_{oc} of 0.78V was obtained, which is far below than that reported by literature.[19] After PEI modification and DMF treatment we obtain an enhanced V_{oc} of 0.88 V and a PCE of 6.75%. We also noted that the DMF treatment worked best in the state-of-the-art PTB7 and PTB7-Th material systems. The V_{oc}, J_{sc}, FF and PCE of best PTB7-Th-based device are increased to 0.79 V, 18.62 mA/cm^2, 70.0% and 10.30%, respectively. This can be explained, by considering that the efficient PTB7-Th active layers can produce more free carriers and are therefore more sensitive to low efficiency extraction. Fig. S4 shows the EQE spectra and corresponding integrated J_{sc} curves based on different active layer system. The integrated J_{sc}s are within 7% of the values obtained from the *J-V* curves, suggesting the reliability of our measurement.

In conclusion, we obtained enhanced solar cell efficiency using a ZnO/PEI cathode buffer layer washed with DMF. When hot DMF solvent is used to wash the PEI surface after deposition, a wider range of processing conditions are found to lead to high efficiency devices. By analyzing the surface topography combined with XPS, PL, FTIR, IS and some transient optoelectronics techniques we concluded that the treatment with DMF results in an interlayer with more uniform and smooth morphology, reduced surface defect states, better

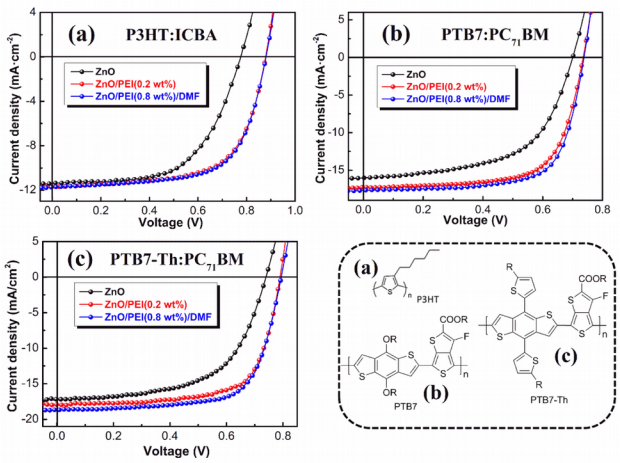

Fig. 11. The *J-V* characteristics of devices based on (a) P3HT:ICBA, (b) PTB7:$PC_{71}BM$ and (c) PTB7-Th:$PC_{71}BM$ material systems.

3. Conclusion

Table 3. Detailed parameters of devices based on P3HT:ICBA, PTB7:$PC_{71}BM$ and PTB7-Th:$PC_{71}BM$ active layer.

active layer	interfacial layer	V_{oc} (V)	J_{sc} (mA/cm^2)	J_{sc}^{EQE} (mA/cm^2)	FF (%)	PCE (%)	
						Max.	Aver.
P3HT:ICBA	ZnO	0.78±0.01	11.24±0.12	10.21(9.7%)	58.5±0.7	5.19	5.12
	ZnO/PEI(0.2 wt%)	0.88±0.01	11.68±0.10	10.60(9.0%)	64.1±0.8	6.66	6.58
	ZnO/PEI(0.8 wt%)/DMF	0.88±0.01	11.74±0.07	10.80(7.6%)	65.0±0.5	6.75	6.71
PTB7:$PC_{71}BM$	ZnO	0.69±0.02	16.03±0.11	14.42(9.8%)	57.7±1.1	6.47	6.38
	ZnO/PEI(0.2 wt%)	0.73±0.01	17.23±0.14	15.56(9.5%)	68.0±0.6	8.61	8.51
	ZnO/PEI(0.8 wt%)/DMF	0.74±0.01	17.66±0.15	16.02(9.1%)	70.0±0.4	9.18	9.12
PTB7-Th:$PC_{71}BM$	ZnO	0.74±0.01	17.08±0.15	15.66(8.4%)	58.4±1.3	7.48	7.34
	ZnO/PEI(0.2 wt%)	0.79±0.01	18.00±0.09	16.52(7.8%)	68.3±0.8	9.86	9.67
	ZnO/PEI(0.8 wt%)/DMF	0.79±0.01	18.47±0.19	17.21(7.5%)	70.0±0.9	10.30	10.16

wetting, lower resistance and improved charge extraction. We finally, show that this method relaxing processing conditions and increasing cell efficiency, is generally applicable to devices containing other state-of-the-art material systems in the active layer. Indeed, the more efficient the material system, the more beneficial DMF washing becomes.

Acknowledgements

This work was supported by the National Natural Science Foundation of China (Grant Nos. 51303061, 11574110), the Project of Science and Technology Development Plan of Jilin Province (Grant Nos. 20140204056GX, 20160204013GX), the Project of Science and Technology Plan of Changchun City (Grant No.13KG49), and the China Postdoctoral Science Foundation (Grant No. 2014T70288, 2013M541299, 2016M600231).

Notes and references

1 G. Yu, J. Gao, J. C. Hummelen, F. Wudl and A. J. Heeger, *Science*, 1995, **270**, 1789-1791.
2 G. Li, V. Shrotriya, J. Huang, Y. Yao, T. Moriarty, K. Emery and Y. Yang, *Nature Mater.*, 2005, **4**, 864-868.
3 J. Brabec, N. S. Sariciftci and J. C. Hummelen, *Adv. Funct. Mater.*, 2001, **11**, 15-26.
4 M. M. Wienk, J. M. Kroon, W. J. H. Verhees, J. Knol, J. C. Hummelen, P. A. van Hal and R. A. J. Janssen, *Angew. Chem. Int. Ed.*, 2003, **115**, 3493-3497.
5 S. P. Wen, J. N. Pei, Y. H. Zhou, P. F. Li, L. L. Xue, Y. W. Li, B. Xu and W. J. Tian, *Macromolecules*, 2009, **42**, 4977-4984.
6 B. Kan, Q. Zhang, M. M. Li, X. J. Wan, W. Ni, G. K. Long, Y. C. Wang, X. Yang, H. R. Feng and Y. S. Chen, *J. Am. Chem. Soc.*, 2014, **136**, 15529-15532.

7 D. Deng, Y. Zhang, J. Zhang, Z. Wang, L. Zhu, J. Fang, B. Xia, Z. Wang, K. Lu, W. Ma and Z. Wei, *Nat. Commun.*, 2016, **7**, 13740.

8 J. Zhao, Y. Li, G. Yang, K. Jiang, H. Lin, H. Ade, W. Ma and H. Yan, *Nature Energy*, 2016, **1**, 15027.

9 B. H. Cumpston and K. F. Jensen, *J. Appl. Polym. Sci.*, 1998, **69**, 2451-2458.

10 Z. Yin, Q. Zheng, S.-C. Chen, D. Cai and Y. Ma, *Adv. Energy Mater.*, 2016, **6**, 1501493.

11 S. A. Gevorgyan, N. Espinosa, L. Ciammaruchi, B. Roth, F. Livi, S. Tsopanidis, S. Züfle, S. Queirós, A. Gregori, G. A. d. R. Benatto, M. Corazza, M. V. Madsen, M. Hösel, M. J. Beliatis, T. T. Larsen-Olsen, F. Pastorelli, A. Castro, A. Mingorance, V. Lenzi, D. Fluhr, R. Roesch, M. Maria Duarte Ramos, A. Savva, H. Hoppe, L. S. A. Marques, I. Burgués, E. Georgiou, L. Serrano-Luján and F. C. Krebs, *Adv. Energy Mater.*, 2016, **6**, 1600910.

12 Y. Liang, Z. Xu, J. Xia, S. T. Tsai, Y. Wu, G. Li, C. Ray and L. Yu, *Adv. Mater.*, 2010, **22**, E135-E138.

13 S.-H. Liao, H.-J. Jhuo, Y.-S. Cheng and S.-A. Chen, *Adv. Mater.*, 2013, **25**, 4766-4771.

14 Y. Liu, J. Zhao, Z. Li, C. Mu, W. Ma, H. Hu, K. Jiang, H. Lin, H. Ade and H. Yan, *Nat. Commun.*, 2014, **5**, 5293.

15 W. Zhao, D. Qian, S. Zhang, S. Li, O. Inganas, F. Gao and J. Hou, *Adv. Mater.*, 2016, **28**, 4734-4739.

16 Z. He, C. Zhong, S. Su, M. Xu, H. Wu and Y. Cao, *Nat. Photonics*, 2012, **6**, 591-595.

17 Z. Xu, L.-M. Chen, G. Yang, C.-H. Huang, J. Hou, Y. Wu, G. Li, C.-S. Hsu and Y. Yang, *Adv. Funct. Mater.*, 2009, **19**, 1227-1234.

18 M. Campoy-Quiles, T. Ferenczi, T. Agostinelli, P. G. Etchegoin, Y. Kim, T. D. Anthopoulos, P. N. Stavrinou, D. D. C. Bradley and J. Nelson, *Nat. Mater.*, 2008, **7**, 158-164.

19 Z. Tan, L. Li, F. Wang, Q. Xu, S. Li, G. Sun, X. Tu, X. Hou, J. Hou and Y. Li, *Adv. Energy Mater.*, 2014, **4**, 1300884.

20 C. Z. Li, C. Y. Chang, Y. Zang, H. X. Ju, C. C. Chueh, P. W. Liang, N. Cho, D. S. Ginger and A. K. Jen, *Adv. Mater.*, 2014, **26**, 6262-6267.

21 J. Meyer, S. Hamwi, M. Kröger, W. Kowalsky, T. Riedl and A. Kahn, *Adv. Mater.*, 2012, **24**, 5408-5427.

22 Z. He, B. Xiao, F. Liu, H. Wu, Y. Yang, S. Xiao, C. Wang, T. P. Russell and Y. Cao, *Nat. Photonics*, 2015, **9**, 174-179.

23 S. Li, L. Ye, W. Zhao, S. Zhang, S. Mukherjee, H. Ade and J. Hou, *Adv. Mater.*, 2016, **28**, 9423-9429.

24 S. Woo, W. Hyun Kim, H. Kim, Y. Yi, H.-K. Lyu and Y. Kim, *Adv. Energy Mater.*, 2014, **4**, 1301692.

25 X. Meng, W. Zhang, Z. Tan, C. Du, C. Li, Z. Bo, Y. Li, X. Yang, M. Zhen, F. Jiang, J. Zheng, T. Wang, L. Jiang, C. Shu and C. Wang, *Chem. Commun.*, 2012, **48**, 425-427.

26 L. Dou, J. You, J. Yang, C. Chen, Y. He, S. Murase, T. Moriarty, K. Emery, G. Li and Y. Yang, *Nature Photonics*, 2012, **6**, 180-185.

27 Z. Liang, Q. Zhang, L. Jiang and G. Cao, *Energy Environ. Sci.*, 2015, **8**, 3442-3476.

28 P. Zhang, J. Wu, T. Zhang, Y. Wang, D. Liu, H. Chen, L. Ji, C. Liu, W. Ahmad, Z. D. Chen and S. Li, *Adv. Mater.*, 2018, **30**, 1703737.

29 Y. Sun, J. H. Seo, C. J. Takacs, J. Seifter and A. J. Heeger, *Adv. Mater.*, 2011, **23**, 1679-1683.

30 T. Yang, M. Wang, C. Duan, X. Hu, L. Huang, J. Peng, F. Huang and X. Gong, *Energy Environ. Sci.*, 2012, **5**, 8208-8214.

31 V. Ischenko, S. Polarz, D. Grote, V. Stavarache, K. Fink and M. Driess, *Adv. Funct. Mater.*, 2005, **15**, 1945-1954.

32 T. Hu, F. Li, K. Yuan and Y. Chen, *ACS Appl. Mater. Interfaces*, 2013, **5**, 5763-5770.

33 Y.-M. Chang and C.-Y. Leu, *J. Mater. Chem. A*, 2013, **1**, 6446-6451.

34 S. Nam, J. Seo, S. Woo, W. H. Kim, H. Kim, D. D. Bradley and Y. Kim, *Nat. Commun.*, 2015, **6**, 8929.

35 K. Zhang, Z. Hu, R. Xu, X. F. Jiang, H. L. Yip, F. Huang and Y. Cao, *Adv. Mater.*, 2015, **27**, 3607-3613.

36 Z. A. Page, Y. Liu, V. V. Duzhko, T. P. Russell and T. Emrick, *Science*, 2014, **346**, 441-444.

37 Y. Zhou, C. Fuentes-Hernandez, J. Shim, J. Meyer, A. J. Giordano, H. Li, P. Winget, T. Papadopoulos, H. Cheun, J. Kim, M. Fenoll, A. Dindar, W. Haske, E. Najafabadi, T. M. Khan, H. Sojoudi, S. Barlow, S. Graham, J. L. Bredas, S. R. Marder, A. Kahn and B. Kippelen, *Science*, 2012, **336**, 327-332.

38 A. K. Kyaw, D. H. Wang, V. Gupta, J. Zhang, S. Chand, G. C. Bazan and A. J. Heeger, *Adv. Mater.*, 2013, **25**, 2397-2402.

39 F. C. Krebs, *Sol. Energy Mater. Sol. Cells*, 2009, **93**, 465-475.

40 S. Wen, C. Wang, P. Ma, Y.-X. Zhao, C. Li and S. Ruan, *J. Mater. Chem. A*, 2015, **3**, 13794-13800.

41 A. Kasprzak, M. Poplawska, H. Krawczyk, S. Molchanov, M. Kozlowski and M. Bystrzejewski, *J. Incl. Phenom. Macrocycl. Chem.*, 2017, **87**, 53-65.

42 B. Lee, S. Lee, J. Park, E. Jung, J. Yu, Y. Nam, J. Heo, J. Kim, B. Kim and M. Song, *Adv. Mater.*, 2015, **27**, 3553-3559.

43 Y. Yan, F. Cai, L. Yang, J. Li, Y. Zhang, F. Qin, C. Xiong, Y. Zhou, D. G. Lidzey and T. Wang, *Adv. Mater.*, 2017, **29**, 1604044.

44 W. Jin, R. Ginting, S. Jin and J. Kang, *J. Mater. Chem. A*, 2016, **4**, 3784-3791.

45 S. Chen, C. E. Small, C. M. Amb, J. Subbiah, T.-h. Lai, S.-W. Tsang, J. R. Manders, J. R. Reynolds and F. So, Adv. Energy Mater., 2012, **2**, 1333-1337.

46 F. Fabbri, M. Villani, A. Catellani, A. Calzolari, G. Cicero, D. Calestani, G. Calestani, A. Zappettini, B. Dierre, T. Sekiguchi and G. Salviati, Sci. Rep., 2014, **4**, 5158.

47 J. Subbiah, B. Purushothaman, M. Chen, T. Qin, M. Gao, D. Vak, F. H. Scholes, X. Chen, S. E. Watkins, G. J. Wilson, A. B. Holmes, W. W. H. Wong and D. J. Jones, *Adv. Mater.*, 2015, **27**, 702-705.

48 C. Wang, C. Li, S. Wen, P. Ma, Y. Liu, R. C. MacKenzie, W. Tian and S. Ruan, *J. Mater. Chem. A*, 2017, **5**, 3995-4002.

49 C. G. Shuttle, N. D. Treat, J. D. Douglas, J. M. J. Fréchet and M. L. Chabinyc, *Adv. Energy Mater.*, 2012, **2**, 111-119.

50 R. C. I. MacKenzie, C. G. Shuttle, M. L. Chabinyc and J. Nelson, *Adv. Energy Mater.*, 2012, **2**, 662-669.

51 A. Maurano, C. G. Shuttle, R. Hamilton, A. M. Ballantyne, J. Nelson, W. Zhang, M. Heeney and J. R. Durrant, *J. Phys. Chem. C*, 2011, **115**, 5947-5957.
52 H. Zhou, Y. Zhang, J. Seifter, S. D. Collins, C. Luo, G. C. Bazan, T. Q. Nguyen and A. J. Heeger, *Adv. Mater.*, 2013, **25**, 1646-1652.
53 R. Hanfland, M. A. Fischer, W. Bruetting, U. Wuerfel and R. C. I. MacKenzie, *Appl. Phys. Lett.*, 2013, **103**, 063904.
54 B. Ecker, H.-J. Egelhaaf, R. Steim, J. Parisi and E. von Hauff, *J. Phys. Chem. C*, 2012, **116**, 16333-16337.
55 G. Garcia-Belmonte, A. Guerrero and J. Bisquert, *J. Phys. Chem. Lett.*, 2013, **4**, 877-886.
56 B. J. Leever, C. A. Bailey, T. J. Marks, M. C. Hersam and M. F. Durstock, *Adv. Energy Mater.*, 2012, **2**, 120.